厚生労働科学研究費補助金（肝炎等克服緊急対策研究事業）
分担研究報告書

ビタミンA 非含有細胞のマーカーについて

研究分担者 武田 憲彦 東京大学医学研究科 助教

研究要旨:

研究要旨:

肝線維症は，肝臓におけるコラーゲンを主とした細胞外基質(ECM)の蓄積であり，この病態反応は、ほぼ全ての原因による慢性肝炎に共通である。慢性肝炎の終末像は肝硬変であり、肝硬変の治療法は肝移植を除けば対症療法のみである。肝線維化の進行を阻止する治療薬を開発することは、医学的にも医療経済上も重要であるが、現在、臨床的に有効な薬剤は存在しない。本研究は、線維化モデル動物を用いた基礎的な解析を基に、肝炎症において誘導されるビタミンA非含有細胞に着目し、肝線維症の新たな治療標的としての可能性を見い出すことを目的とするものである。

A．研究目的

慢性肝炎病態では組織の傷害と修復反応が繰り返されている。持続的な修復反応の一つに、筋線維芽細胞による細胞外マトリクス（extra cellular matrix: ECM）の産生・沈着があるが、肝内での過剰な ECM 沈着には、肝実質細胞の絶対数の減少が伴い、肝機能低下をもたらす。さらに近年、詳細は不明なものの、ECM 沈着 が細胞癌化を促進する可能性も示されている。これらに加え、肝線維化・肝硬変が進行して重篤な肝機能不全に陥ると、現在のところ肝臓機能を人工的に代替する医療は完成されていないため、肝移植しか治療の手立てがない。このため、肝硬変の進行を食い止めることは、患者の QOL を考える上でも、医療経済学的にも大きな意義をもつ。

当該共同研究グループ祝迫、上本、朝霧ら、ならびに カリフォルニア大学 David Brenner らは、Collagen promoter-GFP マウスを用いた実験から、ビタミン A を含有しない細胞系列(非肝星細胞系列)も、肝硬変進行時にコラーゲンを産生しうるという予備知見を得ている。

肝臓の筋線維芽細胞は、慢性肝障害に応じて活性化され、コラーゲンを主体とした ECM を盛んに分泌して組織の線維性瘢痕変性を導く。一方、肝星細胞は、肝傷害時に増殖してコラーゲンを産生することから、慢性肝炎における肝線維化の責任細胞と目されていた。実際、肝硬変治療薬の多くは、肝星細胞を標的として研究が進められてきた経緯がある。しかし、広範の研究にもかかわらず、肝硬変の進行途上で ECM を分泌する細胞(筋線維芽細胞)が、肝星細胞系列だけで構成されているのか否かについては決着がついていない。もし、活性化肝星細胞以外にも、ECM の過剰沈着に関与する細胞があり、肝星細胞とは異なる mode of action で炎症に反応して ECM を産生したり、あるいは肝内で特異的局在を示すとしたら、肝硬変の進行を遮断するための治療ターゲットとなる可能性がある。

我々は、活性化肝星細胞以外の ECM 産生細胞として胆管周囲線維芽細胞の存在に着目し解析を進めている。この細胞系列は、肝硬変の進行を遮断するための治療ターゲットとなる可能性がある。

原疾患による胆汁排泄障害，肝移植を含めた肝胆道系手術後の胆汁鬱滞は，肝線維化を進行させ肝機能を低下させる。ヒトの胆汁鬱滞による肝線維化は，ウイルス肝炎とは異なり，門脈域に優位な線維化を呈する。門脈域にコラーゲン産生細胞が存在することは知られているが，その起源や性質はほとんど明らかになっていない．胆汁鬱

滞の原因を取り除くことが困難な場合，この細胞は肝線維化の治療標的になり得ると考えられる。

B. 研究方法

これまでにビタミンA 非含有細胞外マトリクス産生細胞のマーカーとして同定されたMesothelinについて、臨床検体免疫組織学に門脈域の線維芽細胞のマーカーとしての妥当性を検証してきた。Mesothelinは活性化した門脈域の線維芽細胞に発現が認められたが、正常肝、肝炎、線維化と病態の進展に伴う発現の変化について検討した。

C. 研究結果

臨床検体(胆汁鬱滞性線維肝)の免疫染色では門脈域の線維芽細胞がMesothelin陽性であったが、正常肝、慢性肝炎ではMesothelin陽性細胞は認められなかった。

D. 考察

Mesothelinは、活性化した門脈域の線維芽細胞(＝ビタミンA非含有細胞)には発現が認められるが、静止期では発現が認められないことが分かった。

E. 結論

Mesothelinは、活性化した門脈域の線維芽細胞(＝ビタミンA非含有細胞)のマーカーである。静止期の門脈域線維芽細胞には発現が認められず、活性化の過程で発現誘導される膜タンパクである。

F. 健康危険情報

特に無し。

G. 研究発表

1. 論文発表

Ruthenborg RJ, Ban JJ, Wazir A, Takeda N, Kim JW. Regulation of wound healing and fibrosis by hypoxia and hypoxia-inducible factor-1. Mol Cells. 2014;37(9):637-43.

Abe H, Iguchi N, Utanohara Y, Inoue K, Takamisawa I, Seki A, Tanizaki K, Takeda N, Tohbaru T, Asano R, Nagayama M, Takayama M, Umemura J, Sumiyoshi T, Tomoike H. Non-invasive diagnosis of coronary artery disease by 123I-BMIPP/201TlCl dual myocardial SPECT in patients with heart failure. Int J Cardiol. 2014;176(3):969-74.

Takemoto K, Hatano E, Iwaisako K, Takeiri M, Noma N, Ohmae S, Toriguchi K, Tanabe K, Tanaka H, Seo S, Taura K, Machida K, Takeda N, Saji S, Uemoto S, Asagiri M. Necrostatin-1 protects against reactive oxygen species (ROS)-induced hepatotoxicity in acetaminophen-induced acute liver failure. FEBS Open Bio. 2014;4:777-87.

H. 知的財産研の出願・登録状況

特記すべきことなし。

III. 研究成果の刊行に関する一覧

研究成果の刊行に関する一覧表
【H26. 4. 1～H27. 3. 31】

雑誌

発表者氏名	論文タイトル名	発表誌名	巻号	ページ	出版年
Iwaisako K, Asagiri M et al.	Origin of myofibroblasts in the fibrotic liver in mice.	Proc Natl Acad Sci U S A.	111	E3297-3305	2014
Iwaisako K, Asagiri M et al.	Strategies to Detect Hepatic Myofibroblasts in Liver Cirrhosis of Different Etiologies.	Curr Pathobiol Rep.	2	209-215	2014
Iwaisako K, Uemoto S, Asagiri M et al.	Necrostatin-1 protects against reactive oxygen species (ROS)-induced hepatotoxicity in acetaminophen-induced acute liver failure	FEBS Open Bio.	4	777-787	2014

IV. 研究成果の刊行物・別刷

Origin of myofibroblasts in the fibrotic liver in mice

Keiko Iwaisako[a,b,c,1], Chunyan Jiang[a,c,d,1], Mingjun Zhang[a,1], Min Cong[a,c,d], Thomas Joseph Moore-Morris[e], Tae Jun Park[a], Xiao Liu[a,c], Jun Xu[a,c], Ping Wang[a,c,d], Yong-Han Paik[f], Fanli Meng[a,g], Masataka Asagiri[h], Lynne A. Murray[i], Alan F. Hofmann[a], Takashi Iida[j], Christopher K. Glass[k], David A. Brenner[a], and Tatiana Kisseleva[c,2]

Departments of [a]Medicine, [c]Surgery, and [k]Cellular and Molecular Medicine, and [e]School of Pharmacy, University of California, San Diego, La Jolla, CA 92093; [b]Department of Target Therapy Oncology, Graduate School of Medicine, Kyoto University, Kyoto 606-8507, Japan; [d]Beijing Friendship Hospital, Capital Medical University, Beijing 100050, China; [f]Division of Gastroenterology and Hepatology, Department of Internal Medicine, Samsung Medical Center, Sungkyunkwan University School of Medicine, Seoul 135-710, Korea; [g]Department of Hepatology, Qilu Hospital Shandong University, Shandong 250012, China; [h]Innovation Center for Immunoregulation and Therapeutics, Graduate School of Medicine, Kyoto University, Kyoto 606-8507, Japan; [i]MedImmune Ltd., Cambridge CB21 6GH, United Kingdom; and [j]Department of Chemistry, College of Humanities and Sciences, Nihon University, Sakurajousui, Setagaya, Tokyo 156-8550, Japan

Edited* by Michael Karin, University of California, San Diego School of Medicine, La Jolla, CA, and approved June 23, 2014 (received for review January 6, 2014)

Hepatic myofibroblasts are activated in response to chronic liver injury of any etiology to produce a fibrous scar. Despite extensive studies, the origin of myofibroblasts in different types of fibrotic liver diseases is unresolved. To identify distinct populations of myofibroblasts and quantify their contribution to hepatic fibrosis of two different etiologies, collagen-α1(I)-GFP mice were subjected to hepatotoxic (carbon tetrachloride; CCl_4) or cholestatic (bile duct ligation; BDL) liver injury. All myofibroblasts were purified by flow cytometry of GFP^+ cells and then different subsets identified by phenotyping. Liver resident activated hepatic stellate cells (aHSCs) and activated portal fibroblasts (aPFs) are the major source (>95%) of fibrogenic myofibroblasts in these models of liver fibrosis in mice. As previously reported using other methodologies, hepatic stellate cells (HSCs) are the major source of myofibroblasts (>87%) in CCl_4 liver injury. However, aPFs are a major source of myofibroblasts in cholestatic liver injury, contributing >70% of myofibroblasts at the onset of injury (5 d BDL). The relative contribution of aPFs decreases with progressive injury, as HSCs become activated and contribute to the myofibroblast population (14 and 20 d BDL). Unlike aHSCs, aPFs respond to stimulation with taurocholic acid and IL-25 by induction of collagen-α1(I) and IL-13, respectively. Furthermore, BDL-activated PFs express high levels of collagen type I and provide stimulatory signals to HSCs. Gene expression analysis identified several novel markers of aPFs, including a mesothelial-specific marker mesothelin. PFs may play a critical role in the pathogenesis of cholestatic liver fibrosis and, therefore, serve as an attractive target for antifibrotic therapy.

ECM deposition | markers of fibrogenic myofibroblasts

Chronic liver injury of many etiologies results in liver fibrosis. There are two general types of chronic liver diseases, hepatocellular (injury to hepatocytes, such as chronic viral hepatitis and nonalcoholic steatohepatitis) and cholestatic (obstruction to bile flow, such as primary biliary cirrhosis and primary sclerosing cholangitis) (1). Experimental rodent models of liver fibrosis mimic these two types of chronic liver injuries: Repeated carbon tetrachloride (CCl_4) administration produces hepatocelluar injury, and common bile duct ligation (BDL) produces cholestatic injury (2). In all chronic liver diseases, myofibroblasts are embedded in the fibrous scar and are the source of this excessive extracellular matrix (ECM). Myofibroblasts, which are not present in normal liver, are characterized by distinct morphology, contractility with intracellular stress fibers [α-smooth muscle actin (α-SMA), nonmuscle myosin, and vimentin], and secretion of extracellular matrix (fibronectin and fibrillar collagens) (1, 2).

The cells of origin of hepatic myofibroblasts are unresolved, and perhaps the fibrosis induced by different types of liver injury results from different fibrogenic cells. Hepatic myofibroblasts may originate from bone marrow (BM)-derived mesenchymal cells and fibrocytes, but only a small contribution of BM-derived cells to the myofibroblast population has been detected in experimental liver fibrosis (3–5). Another potential source of myofibroblast is epithelial-to-mesenchymal transition (EMT), in which epithelial cells acquire a mesenchymal phenotype and may give rise to fully differentiated myofibroblasts. However, recent cell fate mapping studies have failed to detect any hepatic myofibroblasts originating from hepatocytes, cholangiocytes, or epithelial progenitor cells (3, 6–10). Thus, the major sources of myofibroblasts in liver fibrosis are the endogenous liver mesenchymal cells, which consist of portal fibroblasts and hepatic stellate cells.

Quiescent hepatic stellate cells (qHSCs) are located in the space of Disse, store retinoids in lipid droplets, and express neural markers, such as glial fibrillary acidic protein (GFAP), synaptophisin, and nerve growth factor receptor p75 (1). In response to injury, qHSCs down-regulate vitamin A-containing lipid droplets and neural markers, and differentiate into α-SMA–expressing myofibroblasts (1, 2). Portal fibroblasts normally comprise a small population of the fibroblastic cells that surround the portal vein to maintain integrity of portal tract. They were first described as "mesenchymal cells not related to sinusoids," and since then have been called "periductular fibroblasts" or portal/periportal mesenchymal cells" (11) and implicated by association in the pathogenesis of cholestatic liver injury. In

Significance

Liver resident activated hepatic stellate cells (aHSCs), and activated portal fibroblasts (aPFs) are the major source of the fibrous scar in the liver. aPFs have been implicated in liver fibrosis caused by cholestatic liver injury, whereas fibrosis in hepatotoxic liver injury is attributed to aHSCs. However, the contribution of aPFs to cholestatic fibrosis is not well characterized because of difficulties in cell purification and the lack of identified aPF-specific markers. We have developed a novel flow cytometry-based method of aPFs purification from the nonparenchymal cell fraction of collagen-α1(I)-GFP mice and have identified potential aPF-specific markers. The goal of this study is to determine whether aPFs contribute to cholestatic liver fibrosis and identify the mechanism(s) of their activation.

Author contributions: K.I., C.J., M.Z., D.A.B., and T.K. designed research; K.I., C.J., M.Z., M.C., T.J.M.-M., T.J.P., X.L., J.X., P.W., Y.-H.P., F.M., L.A.M., and T.K. performed research; M.A., A.F.H., T.I., C.K.G., and D.A.B. contributed new reagents/analytic tools; K.I., C.J., M.Z., M.C., T.J.M.-M., T.J.P., X.L., J.X., Y.-H.P., F.M., M.A., and C.K.G. analyzed data; and D.A.B. and T.K. wrote the paper.

The authors declare no conflict of interest.

*This Direct Submission article had a prearranged editor.

Freely available online through the PNAS open access option.

[1]K.I., C.J., and M.Z. contributed equally to this work.

[2]To whom correspondence should be addressed. Email: tkisseleva@ucsd.edu.

This article contains supporting information online at www.pnas.org/lookup/suppl/doi:10.1073/pnas.1400062111/-/DCSupplemental.

response to chronic injury, portal fibroblasts may proliferate, differentiate into α-SMA–expressing myofibroblasts, and synthesize extracellular matrix (11–14).

The contribution of portal fibroblasts (PFs) to liver fibrosis of different etiologies is not well understood, mainly because of difficulties in isolating PFs and myofibroblasts. The most widely used method of PF isolation from rats is based on liver perfusion with enzymatic digestion followed by size selection (15). Cell outgrowth from dissected bile segments is still used to isolate mouse PFs, and after 10–14 d in culture, PFs undergo progressive myofibroblastic activation (16). The disadvantage of this technique is that it requires multiple passaging and prolong culturing (11). A more physiological method of PF culturing in a precision-cut liver slice is designed to maintain cell–cell and cell–matrix interactions and mimic natural microenvironment of PFs, but it does not enable the study of purified PFs (17). Therefore, only a few markers of PFs are available to identify PFs in the myofibroblast population, including gremlin, Thy1, fibulin 2, interleukin 6 (IL-6), elastin, the ecto-AT-Pase nucleoside triphosphate diphosphohydrolase-2 (NTPD2), and coffilin 1. In addition, the lack of desmin, cytoglobin, α2-macroglobulin, neural proteins (GFAP, p75, synaptophysin), and lipid droplets distinguishes PFs from HSCs (1, 17–21).

Our study uses transgenic reporter mice and new flow cytometry protocols to identify the origin of myofibroblasts and quantify their numbers in two murine models of chronic liver injury (BDL and CCl_4). Our study demonstrates that the origin of the myofibroblasts is determined by the type of liver injury. As previously reported using other methodologies, HSCs are the major source of myofibroblasts in CCl_4 liver injury. In contrast, most of the myofibroblasts at the onset of BDL-induced liver injury originate from activated PFs (aPFs).

Results

BDL- and CCl_4-Induced Liver Fibrosis Is Associated with Activation of Myofibroblasts in Mice. To study activation of hepatic myofibroblasts, Col-GFP mice expressing GFP under control of collagen α1(I) promoter/enhancer (22) were subjected to BDL (20 d) or CCl_4 (1.5 mo) liver injury. Upon activation, hepatic myofibroblasts in these mice are visualized by GFP expression. Development of liver fibrosis was confirmed in Col-GFP mice by hydroxyproline content, Sirius Red staining (Fig. 1 *A* and *B*) and correlated with increased collagen-α1(I) (fold increase 6.1 ± 0.3 and 7.6 ± 0.4 in BDL- and CCl_4-treated vs. control mice) and α-SMA mRNA expression (fold increase 4.2 ± 0.2 and 6.1 ± 0.7 vs. control mice, respectively; Fig. 1*B*). Development of liver fibrosis was also associated with activation of myofibroblasts, demonstrated by Col-GFP expression (6.5 ± 0.4% and 7.8 ± 0.5% of GFP^+ area in BDL- and CCl_4-treated vs. 0.3 ± 0.03% in control mice) and α-SMA expression (Fig. 1*B*). Thus, BDL and CCl_4 induced comparable levels of fibrosis and activation of myofibroblasts in the liver, sufficient to isolate GFP^+ myofibroblasts and determine their composition in response to two different injuries.

Isolation of Myofibroblasts. The reporter Col-GFP mice (22) have been extensively characterized and are widely used to visualize activated myofibroblasts in fibrotic liver, lungs, kidneys, and skin (3–5, 8, 23–36). Expression of GFP in these mice closely correlates with expression of collagen type I protein in hepatic myofibroblasts but is not expressed in endothelial, epithelial, or other cell types (37–39). Using Col-GFP mice we have demonstrated that activated hepatic stellate cells (aHSCs) (GFP^+, vitamin A^+, $Desmin^+$ cells) comprise >92% of myofibroblasts in response to CCl_4-induced or alcohol-induced fibrosis (1, 40).

Analysis of Activated Myofibroblasts by Flow Cytometry. Our strategy to determine the composition of hepatic myofibroblasts is based on characterization of GFP^+ cells in nonparenchymal liver fractions of BDL- and CCl_4-treated Col-GFP mice (which contains all $Col1a1^+$ and $\alpha\text{-}SMA^+$ myofibroblasts; for details, see Fig. S1*A*) (22). Although collagen-α1(I)-GFP is expressed in all activated myofibroblasts (40, 41), expression of vitamin A (Vit.A) droplets in the liver is solely attributed to HSCs (1) (Fig. 2*A*). The cell fate mapping of HSCs [using $GFAP^{Cre} \times Rosa26^{flox\text{-}TmRed\text{-}Stop\text{-}flox\text{-}GFP}$ mice (40); Fig. S1 *B* and *C*] demonstrated that although HSCs down-regulate vitamin A upon activation (aHSCs), vitamin A is still detected in all aHSCs by flow cytometry (autofluorescent signal of vitamin A; Fig. S1*D*). We used flow cytometry to quantify the contribution of aHSCs ($GFP^+Vit.A^+$) and myofibroblasts of other origins ($GFP^+Vit.A^-$) in BDL and CCl_4 injury (Fig. 2*B*). As expected, activation of hepatic myofibroblasts (GFP^+ cells, 100%) was observed only in injured livers (Fig. 2*B*). CCl_4-activated myofibroblasts contained 87 ± 6% $GFP^+Vit.A^+$ and 13 ± 3% $GFP^+Vit.A^-$ cells. In contrast, the nonparenchymal fraction from BDL (20 d) mice consisted of 56 ± 4% $GFP^+Vit.A^+$ and 42 ± 5% $GFP^+Vit.A^-$ myofibroblasts, suggesting that the composition of GFP^+

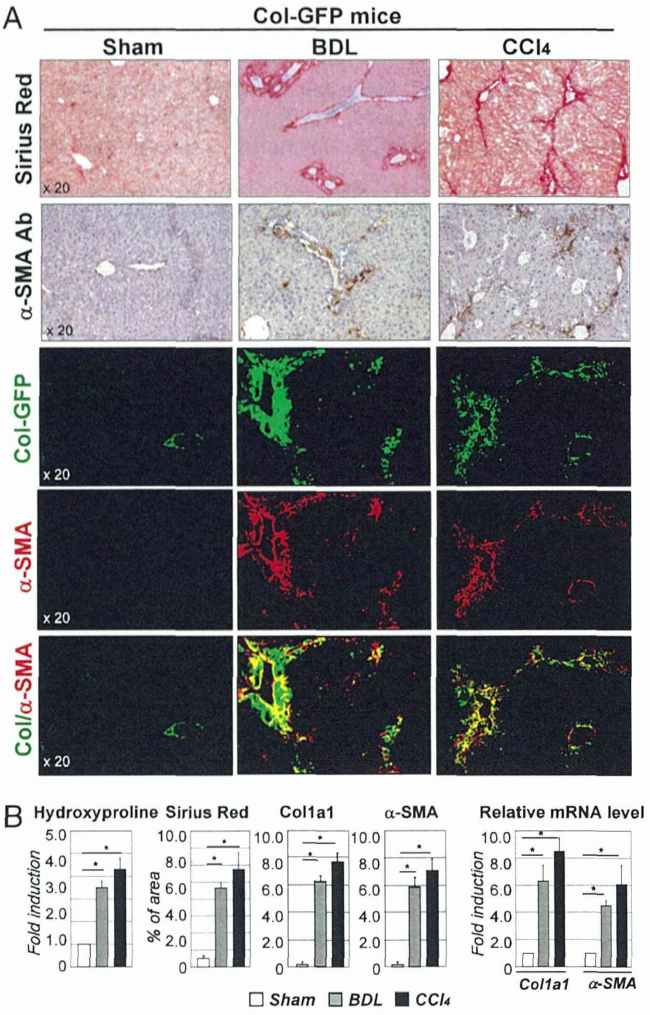

Fig. 1. Development of liver fibrosis in Col-GFP mice in response to BDL and CCl_4. (*A*) CCl_4-treated and BDL-operated mice (but not sham mice, 8-wk-old, $n = 10$ per group) developed liver fibrosis, as shown by Sirius Red staining, fluorescent microscopy for collagen-GFP, and staining for α-SMA (20× objective). (*B*) Fibrosis was assessed by hydroxyproline and Sirius Red (positive area) content and by mRNA levels of fibrogenic genes (Col and α-SMA) in all groups of mice is shown, $^*P < 0.003$; $^{**}P < 0.001$.

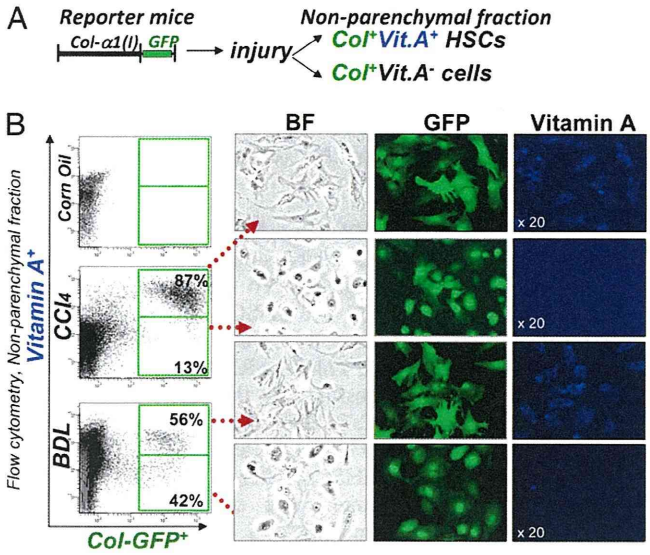

C

GFP+ Myofibroblasts, %		Vit.A+	Vit.A-
CCl_4	5 days	79 ± 3.8	5 ± 2.0
CCl_4	14 days	88 ± 4.0	10 ± 3.6
CCl_4	1.5 mo	87 ± 5.2	13 ± 2.0
BDL	5 days	18 ± 7	73 ± 5
BDL	17 days	45 ± 3	53 ± 4
BDL	20 days	56 ± 4	46 ± 3

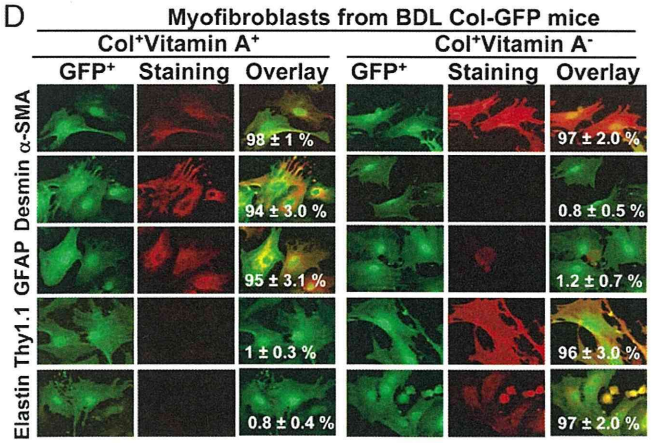

E

GFP+ Myofibroblasts, %		HSCs	aPFs	Others
CCl_4	1.5 mo	83 ± 5.2	13 ± 2.0	4 ± 2.4
BDL	5 day	18 ± 7	73 ± 5	3 ± 2
BDL	17 days	47 ± 3	49 ± 6	4 ± 0.8
BDL	20 days	51 ± 4	43 ± 3	3 ± 1.4

Fig. 2. Detection, quantification, and isolation of liver myofibroblasts. (*A*) Strategy to analyze myofibroblasts by flow cytometry: Collagen type I-expressing myofibroblasts were identified in nonparenchymal fraction by GFP expression and further fractionated to Vit.A$^+$ and Vit.A$^-$ cells. (*B*) FACS analysis of nonparenchymal fraction from untreated and BDL-, and CCl_4-treated Col-GFP mice: GFP$^+$ cells were detected by argon laser at 488 nm wavelength, and Vit.A$^+$ cells were detected by violet laser at 405 nm wavelength. Representative dot plots are shown, $P < 0.03$. GFP$^+$Vit.A$^+$ and GFP$^+$Vit.A$^-$ cells were sort purified and analyzed by light and fluorescent microscopy for GFP and Vitamin A expression (UV laser, 20× objective). (*C*) Flow cytometry-based quantification of GFP$^+$ myofibroblasts. Expression of vitamin A in GFP$^+$ cells was analyzed in nonparenchymal fraction of Col-GFP mice at different time points ($n = 6$ per time point) of CCl_4 and BDL, $P < 0.01$. (*D*) Immunophenotyping of GFP$^+$ myofibroblasts isolated from BDL mice. GFP$^+$Vit.A$^+$ and GFP$^+$Vit.A$^-$ fractions were sort purified from Col-GFP mice ($n = 6$) after BDL (20 d). Expression of myofibroblast marker (α-SMA), HSC markers (desmin, GFAP, CD146), and PF markers (elastin, Thy1) were analyzed by immunocytochemistry using specific antibodies or isotype matched controls (40× objective). GFP$^+$Vit.A$^+$ and GFP$^+$Vit.A$^-$ cells were identified as aHSCs and aPFs, respectively. For each fraction, the percent of positively stained cells is calculated (compared with total cells, 100%, $P < 0.05$). (*E*) Quantification of GFP$^+$Vit.A$^+$ and GFP$^+$Vit.A$^-$ fractions is based on expression of HSC- and PF-specific markers in GFP$^+$ myofibroblasts (100%) as detected by immunocytochemistry, $P < 0.05$.

myofibroblasts varies depending on the etiology of liver fibrosis. GFP$^+$Vit.A$^+$ and GFP$^+$Vit.A$^-$ cells were sort purified and plated (Fig. 2*B*). Expression of GFP was confirmed in both fractions by fluorescent microscopy, whereas expression of Vit.A$^+$ droplets was detected only in GFP$^+$Vit.A$^+$ cells.

Activation of HSCs Differs in BDL- and CCl_4-Induced Liver Injury. Analysis of all GFP$^+$ myofibroblasts (100%) demonstrated that GFP$^+$Vit.A$^+$ aHSCs are the major source of activated myofibroblasts in response to CCl_4 liver injury (Fig. 2*B*). Even at earlier time points of CCl_4 treatment, 79 ± 3% (at 5 d) and 88 ± 4% (at 14 d) of the myofibroblasts were GFP$^+$Vit.A$^+$ HSCs (Fig. S2*A*). In contrast, BDL activated fewer HSCs (Fig. S2*B*). After 5 d of BDL, GFP$^+$ myofibroblasts were mainly composed by GFP$^+$ Vit.A$^-$ cells (73 ± 5%), whereas GFP$^+$Vit.A$^+$ aHSCs represented only 18 ± 7% of GFP$^+$ cells. After BDL (17 d), GFP$^+$ myofibroblasts consisted of 53 ± 4% of GFP$^+$Vit.A$^-$ cells and 45 ± 3% of GFP$^+$Vit.A$^+$ aHSCs, suggesting that activation of HSCs in BDL follows the induction of GFP$^+$Vit.A$^-$ myofibroblasts. Flow cytomery-based statistical analysis of the number of Vit.A$^+$ and Vit.A$^-$ myofibroblasts in response to BDL and CCl_4 is summarized in Fig. 2*C*.

GFP$^+$Vit.A$^+$ Myofibroblast Originate from HSCs, Whereas GFP$^+$Vit.A$^-$ Derive Predominantly from aPFs. Sort-purified GFP$^+$Vit.A$^-$ and GFP$^+$Vit.A$^+$ myofibroblasts were characterized by immunostaining for specific markers. As expected, all GFP$^+$ cells expressed the myofibroblast marker α-SMA, demonstrating that only myofibroblasts express type I collagen in liver fibrosis. BDL-activated GFP$^+$Vit.A$^+$ myofibroblasts expressed the typical HSC markers GFAP (94 ± 2.6%), desmin (98 ± 2%), and mesenchymal marker CD146 (87 ± 3.0%), confirming that the GFP$^+$ Vit.A$^+$ fraction consists solely of aHSCs (Fig. 2*D*). As expected, CCl_4-induced GFP$^+$Vit.A$^+$ myofibroblasts were aHSCs (Fig. S3*A*). In contrast, GFP$^+$Vit.A$^-$ myofibroblasts stained positive for the established portal fibroblast markers Thy1 (93 ± 4.0%) and elastin (86 ± 3.4%), but lacked markers of HSCs (GFAP, Desmin, CD146; Fig. 2*D*) and myeloid cells (CD11b, F4/80, CD68; Fig. S3*B*). Only a small number of GFP$^+$Vit.A$^-$ cells expressed fibrocyte-like markers CD45 (3.1 ± 0.1%) and CD11b (2.4 ± 0.3%; Fig. S3*B*), suggesting that GFP$^+$Vit.A$^-$ fraction predominantly (95 ± 4%) contains aPFs, and that less than 4 ± 1% of myofibroblasts originate from other sources (e.g., fibrocytes and BM derived mesenchymal progenitors). Immunocytochemistry-based analysis of myofibroblast composition in response to both BDL and CCl_4 is summarized in Fig. 2*E*.

Gene Expression Profile Distinguishes BDL-Derived aPFs from CCl_4-aHSCs and BDL-aHSCs. The gene expression profile of BDL-aPFs was compared with BDL-aHSCs and CCl_4-aHSCs (Fig. 3*A*). Using a threshold defining confident detection of gene expression, we confirmed that aPFs exhibited a myofibroblast-like phenotype, sharing mRNA expression of 8,981 genes with aHSCs. These genes included *Col1a1, Col1a2, Col2a1, TIMP-1, Spp1, TGFβ-RI,* and *Vimentin* (Fig. 3*C*) and were induced in aPFs to a level comparable to BDL- and CCl_4-aHSCs. As expected, GFAP and Bambi mRNAs were highly expressed in

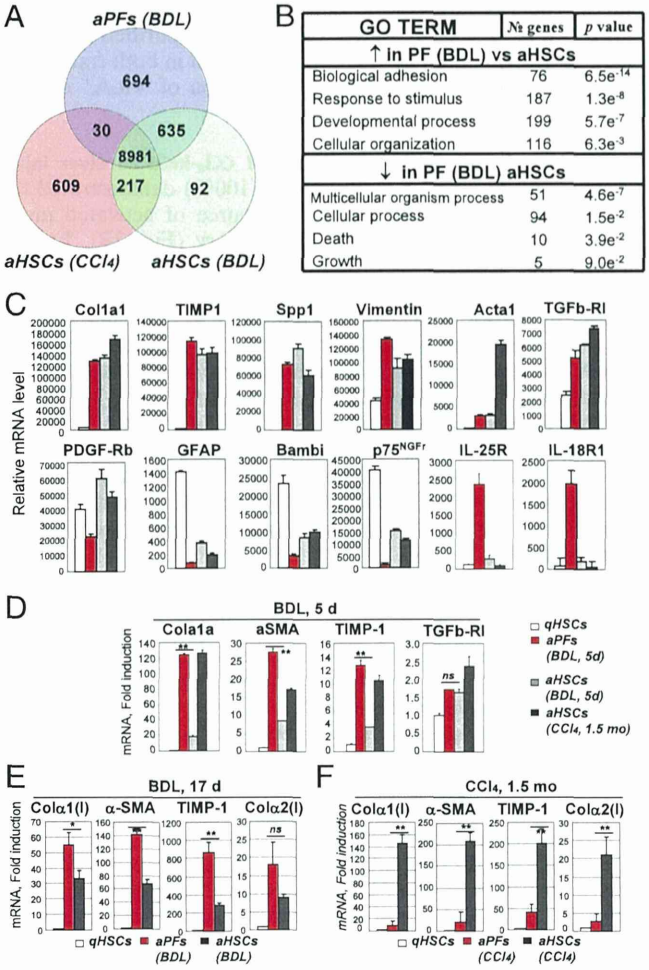

Fig. 3. Characterization of aPFs and aHSCs. (*A*) BDL (20 d) GFP$^+$Vit.A$^-$ aPFs and GFP$^+$Vit.A$^+$ aHSCs were analyzed by the whole mouse genome microarray, and their gene expression profile was compared with that in CCl_4-activated GFP$^+$Vit.A$^+$ HSCs. Venn diagrams of the cell group-enriched genes that exhibited more than a twofold up-regulation compared with other groups. (*B*) GO TERM: demonstrates the signaling pathways that were up-regulated or down-regulated in BDL-aPFs versus BDL- or CCl_4-aHSCs. (*C*) Expression of selected genes in qHSCs, BDL-aHSCs and BDL-aPFs, and CCl_4-aHSCs. The results are relative mRNA level (average of normalized values/multiple probes/per gene) obtained by Agilant microarray, $P < 0.001$. (*D*) Expression of fibrogenic genes was analyzed by RT-PCR in BDL- (5 d) aPFs and BDL-aHSCs, isolated from the same mice ($n = 6$), and compared with that in qHSCs-aHSCs and CCl_4 (1.5 mo)-aHSCs. The data are shown as fold induction compared with qHSCs, $^{**}P < 0.02$ is shown for BDL-aPFs and BDL-aHSCs; ns is not significant. (*E*) Expression of fibrogenic genes was analyzed in BDL (17 d)-aPFs and BDL-aHSCs (isolated from the same mice, $n = 6$) by RT-PCR vs. qHSCs. The data are shown as fold induction compared with qHSCs, $^{*}P < 0.05$; $^{**}P < 0.01$; ns, nonsignificant. (*F*) Similarly, CCl_4- (1.5 mo)aPFs and CCl_4-aHSCs, isolated from the same mice ($n = 4$) were analyzed by RT-PCR. The data are shown as fold induction over qHSCs, $^{*}P < 0.05$; $^{**}P < 0.01$. The data in *D*–*F* represent at least three independent experiments.

qHSCs, whereas *PDGF-Rb* was up-regulated in aHSCs. Meanwhile, the highest expression of *Acta1* was detected in CCl_4-aHSCs (Fig. 3*C*). aPFs up-regulated an additional 694 unique genes (Fig. 3*A*). This set of genes was enriched in Gene Ontology biological process annotations linked to biological adhesion, response to stimulus, developmental process and cellular organization (Fig. 3*B*), locomotion, focal adhesion, cell adhesion molecules, regulation of actin cytoskeleton, and were associated with the induction of the profibrogenic Wnt signaling pathway (Fig. S4). Furthermore, aPFs up-regulated expression of IL-18R, IL-25R (Fig. 3*C*), and other genes that distinguish them from aHSCs (Table 1, discussed below). Interestingly, BDL-aHSCs differentially expressed only 92 genes and shared more similarity with aPFs (635 genes) than with CCl_4-aHSCs (217 genes; Fig. 3*A*), suggesting that in response to cholestatic liver injury, aHSCs may mimic the phenotype of aPFs (for comparison of BDL- and CCl_4-aHSCs, see Fig. S5).

PFs Are Activated in Early BDL-Induced Liver Injury. Our data indicate that aPFs and aHSCs exhibit similar level of activation in response to BDL (20 d; Fig. 3*C*). To further characterize the fibrogenic properties of aPF and aHSC, earlier time points of BDL were examined. After 5 d of BDL (Fig. 3*D*), expression levels of *Col1a1*, *aSMA*, and *TIMP1* mRNA were much higher in aPFs than in aHSCs, suggesting that the activation of PF precedes the activation of HSCs in BDL injury. For example, *Col1a1* was 120-fold induced in aPFs over the level in qHSCs, compared with 20-fold induction in aHSCs. After 17 d of BDL (Fig. 3*E*), activation of HSCs became more prominent (i.e., *Col1a1* mRNA: 33-fold induction in aHSCs, vs. 55 in aPFs). Meanwhile, CCl_4-aPFs exhibited a much lower level of *Col1a1* mRNA than CCl_4-aHSCs (fold induction 20 and 160, respectively; Fig. 3*F*), demonstrating that PFs are only minor contributors to toxic CCl_4-induced liver injury. These data are in concordance with our previous results obtained by flow cytometry (Fig. 2) and

Table 1. Expression of signature genes distinguishes BDL-aPFs from BDL- and CCl_4-aHSCs

Maximum induction (up-regulation) in aPF (BDL, 20 d)	Fold
Calcitonin α (Calca)	66
Glycoprotein m6a (Gpm6a)	35
Uroplakin 1β	28
Basonuclin 1 (Bnc1)	24
Mesothelin (msln)	24
Frizzled-related protein 4 (Sfrp4)	21
Cyp2s1	20
Proteoglycan 4 (Prg4)	18
Asporin (aspn)	18
Mucin 16 (Muc16)	16
IL-18R1	14
Myosin light peptide7 (Myl7)	14
Vitrin (Vit)	12
Glipican 3 (Gpc3)	12
CD200	11
Apolipoprotein D (ApoD)	10
IL-25R	9.7
Dermokin (Dmkn)	9.3
Vanin (Vnn1)	8.5
Thrombospondin 4 (Thbs4)	7.0
Integrin β4 (Itgb4)	6.5
CD55	5.6
Gremlin 1 (Grem1)	4.8
NTPD2	4.6
PDGFc	4.6
Fibulin 2 (Fbln2)	4.4
CD9	3.1
Elastin (Eln)	2.3
Thy1 (CD90)	1.8
Cytoglobin	0.6

Using the whole mouse genome microarray, expression of signature genes was determined for BDL-aPFs. Expression of genes previously identified as PF-specific (underlined) was confirmed. Fold induction (compared with the highest value observed in BDL- or CCl_4-aHSCs) is shown for each gene. Full list of genes is shown in Fig. S7.

demonstrate that there is a correlation between increased number of BDL-aPFs and the level of their activation.

Functional Properties of BDL-Derived aPFs Differ from aHSCs. Previous studies have proposed differences in aPFs and aHSCs that underlie fibrogenesis of different etiologies (42). Therefore, we assessed how aPFs and aHSCs responded to fibrogenic stimuli in vitro. As expected, the fibrogenic cytokine TGF-β1 had similar effects on aPF and aHSC (Fig. 4*A*). However, aPFs were unresponsive to the known HSC agonists PDGF and NGF (demonstrated by mRNA expression of target genes *CyclinD1*; *Bax*, *Bid*, *Bim*, *Bcl-2*, and *Bcl-xl*, respectively). Despite high expression of IL-18R, treatment of aPFs with IL-18 (100 ng/mL; 8 h) did not induce expression of tested IL-18 target genes (*MMP3, MMP8*, and *MMP13, Cox-2, iNOS, IL-6*). Meanwhile, only PFs responded to the bile acid TCA, with increased *Col1a1* mRNA expression (>2.2-fold induction over control aPFs), suggesting that TCA may directly mediate PF activation (Fig. 4*B*). Furthermore, aPFs responded to IL-25 stimulation by induction of IL-13 [similar to IL-13 induction by IL-25–treated macrophages (43) and fibroblasts (44)]. Although IL-13 is implicated in HSC activation, and IL-13 levels are up-regulated in patients with liver cirrhosis (3, 4, 27), the role of IL-13 in cholestatic liver injury has not been well defined. We hypothesize that IL-25–mediated IL-13 production by BDL-aPFs may stimulate activation of HSCs. To assess the effect of aPF-produced IL-13 on HSCs, qHSCs were incubated in the presence of IL-13. As we predicted (45), IL-13 increased *CTCF* (after 4 h) mRNA expression, and also induced up-regulation of *Col1a1*, *aSMA*, *TIMP1*, and mRNA (after 24 h) in HSCs (Fig. 4*C*), suggesting that aPFs may locally facilitate HSC activation via production of IL-13. A more detailed analysis (Fig. 4*D*) demonstrated that stimulation of HSCs with IL-13 causes up-regulation of IL-13Ra2 expression (but not IL-13Ra1 or IL-4) and transcription of IL-13 target genes *Tenascin-C* and *Eotaxin* (46, 47). Because IL-13–treated HSCs did not express IL-13 or IL-6, we concluded that IL-13 directly mediated HSC activation, and this effect was associated with phosphorylation of ERK1/2 (which is completely blocked by ERK inhibitor U0126; Fig. 4*E*) and activation of the p38 and Smad1/5 signaling pathways. Similar results were obtained in human primary HSCs. hIL-13 induced a dose-dependent secretion of CCL11/eotaxin (Fig. S6*A*) in hHSCs. In a separate experiment, hIL-13 alone (or in combination with TGF-β1) mediated an increase in IL-13Ra2, *Tenascin C*, *Col1a1*, *Col3a1*, *fibronectin*, and *LoxL2* genes (Fig. S6*B*). In turn, TGF-β1 and serum stimulation did not result in IL-13 secretion by hHSCs (Fig. S6*C*), suggesting that aPFs may serve as a source of IL-13 in liver fibrosis.

Expression of Novel Markers Distinguishes BDL-Derived aPFs from BDL-aHSCs and CCl_4-aHSCs. To further distinguish aPFs from aHSCs and other myofibroblasts, we interrogated the whole mouse genome microarray to determine "signature genes" for aPFs (Table 1). In concordance with previous studies, we confirmed that aPFs lack expression of cytoglobin (an HSC marker), but express Thy1, elastin, Gremlin 1, Fibulin 2, and NTPD2 mRNAs (the markers that have been reported to discriminate between aPFs and aHSCs) (2, 11, 17–21). However, expression of cofilin-1 (21) distinguished aPFs from CCl_4-aHSCs, but not from BDL-aHSCs, which limits the usefulness of this marker. Furthermore, aPFs uniquely expressed calcitonin α (fold induction >48 over the highest value in BDL-aHSCs or CCl_4-aHSCs), mesothelin (>28), uroplakin 1β (>22), basonuclin 1 (>18), asporin (>14), proteoglycan 4 (>14), glipican 3 (>12), and CD200 (>11) mRNA (Fig. S7). Up-regulation of these genes specifically in aPFs [but not in quiescent or aHSCs, endothelial cells, Kupffer cells, and hepatocytes (Fig. 5*A* and Fig. S8*A*) or BDL-activated cholangiocytes (Fig. 5*A* and Fig. S8*C*)] was confirmed by RT-PCR and immunohistochemistry, suggesting that these genes may serve as potential novel markers of aPFs. Some of these genes (including *basonuclin 1, glycoprotein m6a, uroplakin 3b and 1b, mesothelin, IL-18R, calcitonin-related peptides,* and *vitrin*) were reported as signature genes of murine hepatic mesothelial (48) and epicardial cells (49) (Fig. S7), supporting the theory that PFs originate from mesothelial cells (50, 51).

The role of most of these genes in liver fibrosis has not been evaluated, with the exception of calcitonin α and mesothelin. Calcitonin α, a calcium metabolism regulating hormone, was implicated in pathogenesis of cholestatic injury, and mice devoid of calcitonin α are more resistant to BDL-induced liver fibrosis (52). In turn, mesothelin, a glycosylphosphatidylinositol-linked glycoprotein, is expressed in hepatic mesothelial cells and malignant mesotheliomas (53) and mediates intracellular adhesion and metastatic spread (54). Mesothelin knockout mice are viable and exhibit no obvious abnormalities (55). Expression of mesothelin was detected only in isolated aPFs but not in other cellular fractions (Fig. 5*A*).

Expression of Mesothelin Is Up-Regulated in aPFs in Response to Injury. We examined the expression of mesothelin in isolated aPFs and aHSCs. Unlike GFP^+GFAP^+ aHSCs, GFP^+ aPFs expressed mesothelin (97 ± 1.7%). $Mesothelin^+$ aPFs coexpressed elastin (detected with TE-7 Ab) and Thy1, and immunostaining with mesothelin colocalized with $Elastin^+Thy1^+$ aPFs (Fig. 5*B* and Fig. S8*B*). Next, expression of mesothelin was evaluated in livers of BDL- and CCl_4-injured mice (Fig. 5*C* and Fig. S8*B*). In concordance with our previous findings, very few $mesothelin^+$ cells were detected in CCl_4-injured livers. In contrast, mesothelin was highly expressed in livers from BDL-injured mice, with an expression pattern similar to the other PF markers Thy1 and elastin (Fig. S8 *B* and *C*). In support of our findings, expression of mesothelin mRNA was also detected in laser capture microdissected portal areas from BDL (20 d)-treated mice but not from CCl_4-treated mice (Fig. 5*D*). In addition, mesothelin was not expressed in sham-operated mice, suggesting that mesothelin identifies the aPF phenotype.

Discussion

Our study was designed to determine the origin of hepatic myofibroblasts activated in response to chronic injury of two different etiologies. We demonstrate that hepatotoxic (CCl_4) and cholestatic (BDL) liver injuries activate distinct subsets of fibrogenic myofibroblasts. Thus, CCl_4 activates preferentially aHSCs, whereas BDL initially preferentially aPFs. We developed a reliable method of isolation and quantification of hepatic myofibroblast fractions by using flow cytometry. Based on the distinctive expression of Vitamin A and GFAP in HSCs and Thy1 and elastin in PFs, this study establishes cell sorting as a robust method to purify distinct populations of myofibroblasts in mice, providing a nonbiased approach to purify and characterize all myofibroblasts. By demonstrating that HSCs are the major source of myofibroblasts in hepatotoxic liver injury (CCl_4), we confirmed the previous cell fate mapping studies that used GFAP-Cre (56, 57), PDGFRb-Cre (58), and Lrat-Cre (59).

In contrast to CCl_4-induced injury, our study demonstrates that PFs rapidly activate at the onset of cholestatic injury and up-regulate fibrogenic genes. Furthermore, early activation of PFs during BDL injury may affect HSCs, and BDL-aHSCs exhibit more similarity to aPFs than to CCl_4-aHSCs. Gene expression profiling demonstrated novel signature genes for aPFs. According to cell fate mapping, PFs originate from the mesothelium (51, 60), and our data suggest that aPFs share similarity in signature gene expression with other cells of mesothelial origin. One of these genes, mesothelin, is highly induced specifically in aPFs in response to BDL injury, suggesting that mesothelin may become a new target for antifibrotic therapy.